GeroScience
https://doi.org/10.1007/s11357-024-01339-1

ORIGINAL ARTICLE

Local molecular and connectomic contributions of tau-related neurodegeneration

Fardin Nabizadeh · for the Alzheimer's disease Neuroimaging Initiative (ADNI)

Received: 4 June 2024 / Accepted: 3 September 2024

Abstract Neurodegeneration in Alzheimer's disease (AD) is known to be mostly driven by tau neurofibrillary tangles. However, both tau and neurodegeneration exhibit variability in their distribution across the brain and among individuals, and the relationship between tau and neurodegeneration might be influenced by several factors. I aimed to map local molecular and connectivity characteristics that affect the association between tau pathology and neurodegeneration. The current study was conducted on the cross-sectional tau-PET and longitudinal T1-weighted MRI scan data of 186 participants from the ADNI dataset including 71 cognitively unimpaired (CU) and 115 mild cognitive impairment (MCI) individuals. Furthermore, the normative molecular profile of a region was defined using neurotransmitter receptor densities, gene expression, T1w/T2w ratio (myelination), FDG-PET (glycolytic index, glucose metabolism, and oxygen metabolism), and synaptic density. I found that the excitatory-inhibitory (E:I) ratio, myelination, synaptic density, glycolytic index, and functional connectivity are linked with deviation in the relationship between tau and neurodegeneration. Furthermore, there was spatial similarity between tau pathology and glycolytic index, synaptic density, and functional connectivity across brain regions. The current study demonstrates that the regional susceptibility to tau-related neurodegeneration is associated with specific molecular and connectomic characteristics of the affected neural systems. I found that the molecular and connectivity architecture of the human brain is linked to the different effects of tau pathology on downstream neurodegeneration.

Keywords Alzheimer's disease · Tau · Neurodegeneration · Molecular · Connectivity · Mild cognitive impairment

Data used to prepare this article were obtained from the Alzheimer's disease Neuroimaging Initiative (ADNI) database (adni.loni.usc.edu). As such, the investigators within the ADNI contributed to the design and implementation of ADNI and/or provided data but did not participate in the analysis or writing of this report. A complete listing of ADNI investigators can be found at: http://adni.loni.usc.edu/wp-content/uploads/how_to_apply/ADNI_Acknowledgement_List.pdf.

F. Nabizadeh (✉)
School of Medicine, Iran University of Medical Sciences, Tehran, Iran
e-mail: fardinnabizade1378@gmail.com

F. Nabizadeh
Alzheimer's Disease Institute, Tehran, Iran

Introduction

Alzheimer's disease (AD) is widely known to initiate through the aggregation of amyloid-β (Aβ) within the brain, followed by the accumulation of neocortical tau pathology [1]. This cascade is believed to lead to synaptic dysfunction, cerebral atrophy, and a progressive decline in cognitive function [2, 3]. However,

Published online: 30 September 2024

the exact sequence and interactions among the pathophysiological processes and structural brain changes occurring throughout this prolonged pre-dementia interval remain inadequately understood. AD causes cognitive decline that exhibits significant inter-individual variability in clinical manifestations, as well as in the burden and distribution of pathology [4, 5]. This clinicopathologic heterogeneity offers both challenges and opportunities for systematic, biomarker-driven research aimed at enhancing our understanding of AD biology, diagnostic processes, and treatment strategies.

In a transition toward a biological, rather than clinical, definition of AD, the National Institute on Aging–Alzheimer's Association (NIA-AA) has recently established a biomarker-driven classification known as the A/T/(N) framework [1]. These criteria designate labels indicating the presence (+) or absence (−) of beta-amyloid plaques (A), tau-based neurofibrillary tangles (T), and neurodegeneration (N). Neurodegeneration in AD is known to be mostly driven by tau neurofibrillary tangles, with substantial research supporting a robust spatial and quantitative correlation between measures of tau and neurodegeneration [6–8]. Nevertheless, both tau and neurodegeneration exhibit variability in their distribution across the brain and among individuals, and the relationship between tau pathology and neurodegeneration is not defined by a complete one-to-one correspondence. Compared to the typical association between the deposition of neurofibrillary tangles and neurodegeneration, a divergence in the relationship between tau and neurodegeneration can occur when patients exhibit less neurodegeneration than expected based on their tau levels (indicative of resilience to tau) or more neurodegeneration than expected given their T levels (indicative of susceptibility). The assessment of this disparity could provide insights into resilience and susceptibility in neuronal metabolic reactions to tau. Thus, discrepancies between tau and neurodegeneration may be the effect of additional modulators. Previous studies demonstrated that the association between tau and neurodegeneration is likely attributed to non-AD pathologies or molecular signatures [9, 10]. Also, it has been determined that local molecular and connectivity features of the brain can be involved in susceptibility or resilience to AD pathology [11–16]. The deviation from the normal relationship between tau pathology and downstream neurodegeneration might be due to multiple underlying factors such as age and white matter abnormalities [4]. Capturing the tau pathology and neurodegeneration mismatch can reveal that phenotypes provide a personalized approach for cohort selection in trials and identify the other contributors of neurodegeneration besides tau pathology [4, 17].

The effect of disease can also be influenced by local cellular and molecular susceptibilities. Specifically, regional variations in gene expression [11], neurotransmitter receptor profiles [18], synaptic features [19], metabolism, and connectivity [20] may predispose certain brain regions to stress and subsequent pathology. It is critical to recognize that local and systemic vulnerabilities are not necessarily exclusive of one another; AD may originate from localized pathologies that subsequently propagate selectively across neural networks to other susceptible areas.

Here, I aimed to map local molecular and connectivity attributes of tau pathology and neurodegeneration. I hypothesize that regional molecular and connectivity fingerprints can affect the association between tau and downstream neurodegeneration. The discrepancies between tau and neurodegeneration pose challenges for the application of AD-targeted therapeutics. As the development of disease-modifying therapies progresses, there remains ongoing debate concerning which patients are most likely to benefit from these interventions and to what degree targeting AD-specific pathology will effectively mitigate cognitive decline and neurodegeneration. A precision medicine approach that distinctly quantifies the impact of local molecular and connectivity on tau-related neurodegeneration is crucial as these therapies transition into clinical practice and for patient stratification in clinical trials. In the current study, I first investigated the spatial similarity between the patterns of regional molecular and connectivity fingerprints with tau pathology and longitudinal neurodegeneration separately. In the next step, I create a map of the association between tau pathology and neurodegeneration at each region to investigate the related local molecular and connectivity features.

Methods

Participants

The ADNI study, launched in 2003 as a collaboration between public and private sectors, aims to

determine if a combination of MRI, PET scans, biological markers, and clinical assessments can track the progression of mild cognitive impairment (MCI) and early Alzheimer's disease. More information can be found at www.adniinfo.org. The current study utilized data from ADNI3 (NCT02854033) and was approved by relevant ethics boards. Informed consent was obtained from all participants who were compensated for their involvement. From the ADNI database, 192 participants with baseline tau-PET and longitudinal T1-weighted MRI to obtain cortical thickness data were selected for the study out of 783 individuals with tau-PET. Excluding 6 participants diagnosed with AD dementia due to the small sample size, the final sample of 186 included individuals with either normal cognitive function (CU) or MCI. Clinical status was determined by ADNI criteria: CU participants had an MMSE score above 24, a CDR score of 0, and no depression, while MCI participants had an MMSE score above 24, a CDR score of 0.5, and memory impairment based on the Wechsler Memory Scale II and preserved activities of daily living.

Image processing

The standardized protocols for [18F]Flortaucipir PET imaging were followed at all ADNI sites. Images were captured in 4×5-min frames between 80 and 100 min after injecting approximately 370 MBq of [18F]Flortaucipir. A total of 253 (35%) participants had [18F]Flortaucipir PET scans, conducting a median of 5.2 years (IQR 4.2, 6.1) after their baseline [18F]Florbetapir PET scans, allowing for the assessment of tau pathology at a later time point. Among these participants, 110 had a follow-up scan after 1.3 years (IQR 1.0, 2.1). The analysis utilized Freesurfer-defined Desikan-Killiany atlas regions provided by ADNI, which were generated by aligning the [18F] Flortaucipir image with a previously segmented MRI scan from the same session [21]. I obtained standardized uptake value ratios (SUVRs) of 68 cortical regions to cover the full spectrum of the brain.

The ADNI dataset included standard 3T baseline T1-weighted images. Further details on the acquisition parameters can be found in Jack Jr. et al. [22]. The structural T1-weighted gradient echo pulse sequence data were acquired in sagittal orientation with dimensions of 170×256×256 mm and a voxel resolution of 1.2×1×1 mm. The repetition time was 2300 ms, echo time 2.95 ms, flip angle 9°, and slice thickness 1.2 mm. T2 FLAIR images had dimensions of 175×256×256 with a voxel resolution of 0.9×0.9×5, repetition time 9000 ms, echo time 90 ms, flip angle 150°, and slice thickness 5 mm.

FreeSurfer version 5.3.0 (http://surfer.nmr.mgh.harvard.edu) was used to analyze the MRI data and calculate cortical thickness measurements. The methods for cortical reconstruction and volumetric segmentation using FreeSurfer have been detailed in previous publications [23]. After processing, all images were visually inspected, and any errors in automatic skull stripping or gray/white matter boundary estimation were corrected before reanalyzing. Cortical thickness measures were displayed on the white matter border or the inflated surface of each participant's reconstructed brain to enhance visualization without the influence of cortical folding. The maps were smoothed using a circularly symmetric Gaussian kernel with a FWHM of either 20 mm or 10 mm and then averaged across participants using a non-rigid high-dimensional spherical averaging technique to align cortical folding patterns. This method ensured precise matching of morphologically similar cortical regions across participants, based on their individual anatomy, while reducing metric distortion. As a result, a mean measure of cortical thickness was obtained at each point on the reconstructed surface. The longitudinal cortical thickness of participants with more than one visit (two or four follow-up visits) was included in the current study. I calculated the slope of cortical thickness using linear mixed-effect models with random slope and intercept which were fitted for each brain region, with cortical thickness as the dependent variable and time in years from the baseline scan date as the independent variable.

Molecular and connectomic profile

A total of 10 molecular and connectomic features were used in the analytical models to represent the effect of local molecular and connectomic fingerprints.

Gene expression gradient

The gene gradient across the left cortex, represented by the first principal component of gene expression (PC1), is linked to cell type distributions and

cell-specific gene expression, indicating its connection to the brain's cellular architecture [24, 25]. Data on gene expression was obtained from the Allen Human Brain Atlas and processed using the open-source Python toolbox Abagen [24]. A total of 11,560 genes with differential stability above 0.1 were kept in the region by gene matrix [26]. The left gene gradient was also observed in the right hemisphere. Further details on the processing methods can be found in Hansen et al.'s study [25].

Receptor gradient

The receptor gradient, representing the variation in receptor densities across the cortex, was determined using the first principal component analysis. Receptor densities were estimated through PET tracer studies for a total of 18 receptors and transporters across 9 neurotransmitter systems, including dopamine, norepinephrine, serotonin, acetylcholine, glutamate, GABA, histamine, cannabinoid, and opioids. Volumetric PET images were aligned to the MNI-ICBM152 template and parcellated into 68 cortical regions. The parcellated PET maps were *z*-scored and compiled into a region × receptor matrix of relative densities, as presented in Hansen et al. [27].

Excitatory-inhibitory ratio

The excitatory-inhibitory (E:I) ratio was calculated by comparing the *z*-scored densities of PET-derived excitatory and inhibitory neurotransmitter receptors in the cortex. This analysis utilized the same dataset that was used to calculate the receptor gradient. Excitatory neurotransmitter receptors taken into account were 5-HT2A, 5-HT4, 5-HT6, D1, mGluR5, α4β2, and M1. Inhibitory neurotransmitter receptors considered were 5-HT1A, 5-HT1B, CB1, D2, GABAA, H3, and MOR.

Glycolytic index

Aerobic glycolysis is the process of converting glucose to lactate in the presence of oxygen. Instead of using the traditional ratio of oxygen metabolism to glucose metabolism, we utilize the glycolytic index as a measurement of aerobic glycolysis. The glycolytic index is determined by fitting glucose metabolism to oxygen metabolism in a linear regression model, with larger values indicating more aerobic glycolysis. It is important to note that the glycolytic index and the traditional ratio are highly correlated [28]. Data was collected and analyzed by Vaishnavi et al. [28], with glucose metabolism determined as outlined below and oxygen metabolism measured in participants using labeled water, carbon monoxide, and oxygen. All experiments were conducted with approval from the Human Research Protection Office and the Radioactive Drug Research Committee at Washington University in St. Louis, with written informed consent from all participants.

Glucose metabolism

The study involved measuring glucose metabolism in the cortex of 33 healthy adults (19 female, average age 25.4 ± 2.6 years) through the administration of 18F-labeled fluorodeoxyglucose (FDG) for a PET scan, following the protocol outlined in Vaishnavi et al. [28]. Approval for all experiments was obtained from the Human Research Protection Office and the Radioactive Drug Research Committee at Washington University in St. Louis, with written informed consent provided by all participants.

Synapse density

Synapse density in the cortex was assessed in a group of 76 healthy adults, consisting of 45 males with an average age of 48.9 ± 18.4 years. The measurement was conducted using ^{11}C-UCB-J, a PET tracer that binds to the synaptic vesicle glycoprotein 2A (SV2A) [29–40]. Data was collected over a 90-min period post-injection using an HRRT PET camera. The non-displaceable binding potential (BPND) was determined using the SRTM2 model, with the centrum semiovale as the reference region and a fixed k0 value of 0.027 (population average). All participants provided written informed consent, and the study was carried out in accordance with protocols approved by the Yale University Human Investigation Committee and the Yale New Haven Hospital Radiation Safety Committee.

Myelination

The T1w/T2w ratios, which are indicative of intracortical myelin levels, were measured using data

from the Human Connectome Project (HCP, S1200 release) for 417 unrelated participants (age range 22–37 years, 193 males) [41, 42]. This study was approved by the WU-Minn HCP Consortium. The imaging data was obtained using a Siemens Skyra 3T scanner, with a T1-weighted MPRAGE sequence and a T2-weighted SPACE sequence, both at an isotropic resolution of 0.7 mm. More information on the imaging protocols and procedures can be found at http://protocols.humanconnectome.org/HCP/3T/imaging-protocols.html.

Image processing involves correcting gradient distortion caused by non-linearities, bias field distortions, and aligning images to a standard reference space. The T1w/T2w ratios for each participant were provided in the surface-based CIFTI file format and segmented into 68 cortical regions based on the Lausanne anatomical atlas [43]. It is important to note that the T1w/T2w ratio is an MRI-based estimate of myelin content that has not yet been validated against myelin histology [44]. Other MRI-based measures, such as magnetization transfer or simultaneous tissue relaxometry of R1 and R2 relaxation rates and proton density (SyMRI), have been validated using myelin histology and are highly correlated [44]. Furthermore, PET imaging may offer a promising approach for mapping myelin content in the brain [45, 46].

Functional connectivity

To explore the potential effect of functional brain connectivity on tau pathology and neurodegeneration, I utilized a template functional connectivity matrix generated from 69 CU individuals in the ADNI cohort who tested negative for Aβ and exhibited low tau-PET binding (global SUVR < 1.3). The methodology for creating the template matrix has been detailed in previous literature [47]. In summary, functional images were processed through realignment, co-registration with native T1 images, detrending, band-pass filtering (0.01–0.08Hz), and nuisance covariate regression (including white matter and CSF signal averages and motion parameters). Frames with excessive displacement (greater than 1 mm) were removed, and only participants with less than 30% censored data were included. Functional connectivity matrices were constructed based on the Desikan-Killiany atlas comprising 68 cortical regions. Fisher-z correlations were calculated between time-series data from voxels within each region of interest to evaluate individual functional connectivity strength metrics. These individual matrices were then averaged and thresholded at 30% density for further analysis.

Statistical analysis

All statistical analyses were performed with R version 4.2.0 (www.R-project.org). For comparing the parametric and non-parametric demographical and clinical variables between MCI and CN groups, the t-test and Mann–Whitney U-test were used, respectively. Initially, I measured the level of spatial similarity using linear regression between the tau-PET SUVR and cortical thickness slope in each ROI across all participants. This process resulted in a map of R^2 values (tau-PET SUVR vs. longitudinal cortical thickness) which describes the level of variance in neurodegeneration explained by tau pathology. The results were considered significant, at a p-value < 0.05 after FDR correction. Next, I measured the association between the tau-PET SUVR and cortical thickness slope at the individual level by applying linear regression analysis between the average values of all regions in each participant.

I assessed whether molecular and connectomic profiles are associated with patterns of tau pathology and neurodegeneration. To that end, using linear regression analysis, I tested the spatial similarity between each molecular and connectomic profile with averaged tau-PET SUVR or cortical thickness slope for all participants. Next, in order to investigate the spatial similarity between molecular and connectomic profiles with tau-explained neurodegeneration (R^2 value), I performed linear regression analysis between each molecular and connectomic profile with R^2 value across all participants.

To create brain maps that show the influence of molecular or connectomic features on tau pathology, neurodegeneration, and tau-explained neurodegeneration, I first measured the residuals using linear regression models of single molecular or connectomic profile as independent and neuroimaging-only (tau pathology, neurodegeneration, and tau-explained neurodegeneration) as dependent variable. The residuals were standardized across regions. The standardized residuals for each region across participants were combined, and the Wilcoxon rank-sum statistic was calculated between

the residuals as the distribution of the residuals did not follow a normal pattern. A null distribution of the Wilcoxon statistic was established by repeating the previous steps with 1000 randomly permuted receptor maps for each imaging modality and receptor. The significance of the Wilcoxon maps for each model was determined by calculating the *z*-scores of the Wilcoxon statistic to its null distribution.

Results

Sample characteristics

The current study was conducted on the cross-sectional tau-PET and longitudinal T1-weighted MRI scan data of 186 participants from the ADNI dataset including 71 CU and 115 MCI individuals in order to explore molecular and connectomic fingerprints of tau-explained neurodegenration (Fig. 1A). The summarized clinical and demographical characteristics of the participants are reported in Table 1. The cortical thickness slope was used as a measure of longitudinal neurodegeneration and derived from a linear mixed-effect model for 68 cortical regions.

To investigate whether the tau-related neurodegeneration pattern is influenced by microarchitectural attributes and network connectivity, I defined molecular and connectivity fingerprints for each of the 68 regions of the Desikan-Killiany atlas [48]. The molecular profile of a region was defined using neurotransmitter receptor densities, gene expression, T1w/T2w ratio (myelination), FDG-PET (glycolytic index, glucose metabolism, and oxygen metabolism), and synaptic density (Fig. 1B and C). Likewise, I defined connectivity fingerprint as the strength of functional connectivity of a given region to all other cortical regions (Fig. 2).

Linear regression models were used to explore the association between tau-PET SUVR and cortical thickness slope with CSF biomarkers including Aβ, p-tau, and total tau and FDG-PET in meta-ROIs. Based on the results, there was a significant association between each of the CSF biomarkers and FDG-PET in meta-ROIs with tau-PET SUVR and cortical thickness slope among our participants (Fig. 3A and B).

Tau accumulation explains the variance in neurodegeneration

In the first step, I tested whether higher cortical tau accumulation was associated with reduced cortical thickness over time across spatially corresponding regions. To this end, I used linear regression models and measured tau-PET SUVR and cortical thickness slope association in each given region across participants. Across all participants, tau-PET SUVR was negatively associated with cortical thickness slope most ($R^2 = 0.086$) prominently in temporal regions (Fig. 4A). On average, across 19 regions that survived the multiple comparison correction, the estimate of R^2 was 0.041 which revealed that tau accumulation explains the variance in neurodegeneration (cortical thickness). Next, I applied the regression analysis at the individual level, where I found that higher baseline tau-PET is associated with faster cortical thinning ($\beta = -0.411$, p-value < 0.001) (Fig. 4B and C).

Molecular and connectomic features are associated with tau pathology and neurodegeneration spatial patterns

An important modifier of tau pathology and neurodegeneration is the regional molecular and connectivity characteristics [49–54]. Therefore, I aimed to investigate whether there are spatial similarities between molecular and connectomic fingerprints with tau pathology and neurodegeneration. I performed linear regression analysis between the spatial group-averaged tau-PET and spatial molecular and connectomic profiles. Based on the analyses, I found that regions with higher glycolytic index exhibit higher tau accumulation ($\beta = 0.399$, p-value $= 0.001$) (Fig. 5A). Also, there was spatial similarity between higher synaptic density and lower tau pathology ($\beta = -0.403$, p-value < 0.001) (Fig. 5B). Furthermore, I found a significant positive association between functional connectivity and tau-PET SUVR ($\beta = 0.520$, p-value < 0.001) (Fig. 5C).

Further, investigating the same relations for longitudinal neurodegeneration (cortical thickness), the strong effect of the glycolytic index and functional connectivity was found on cortical thickness slope (Fig. 5D and E). I found that regions with higher glycolytic index and functional connectivity have slower cortical atrophy over time.

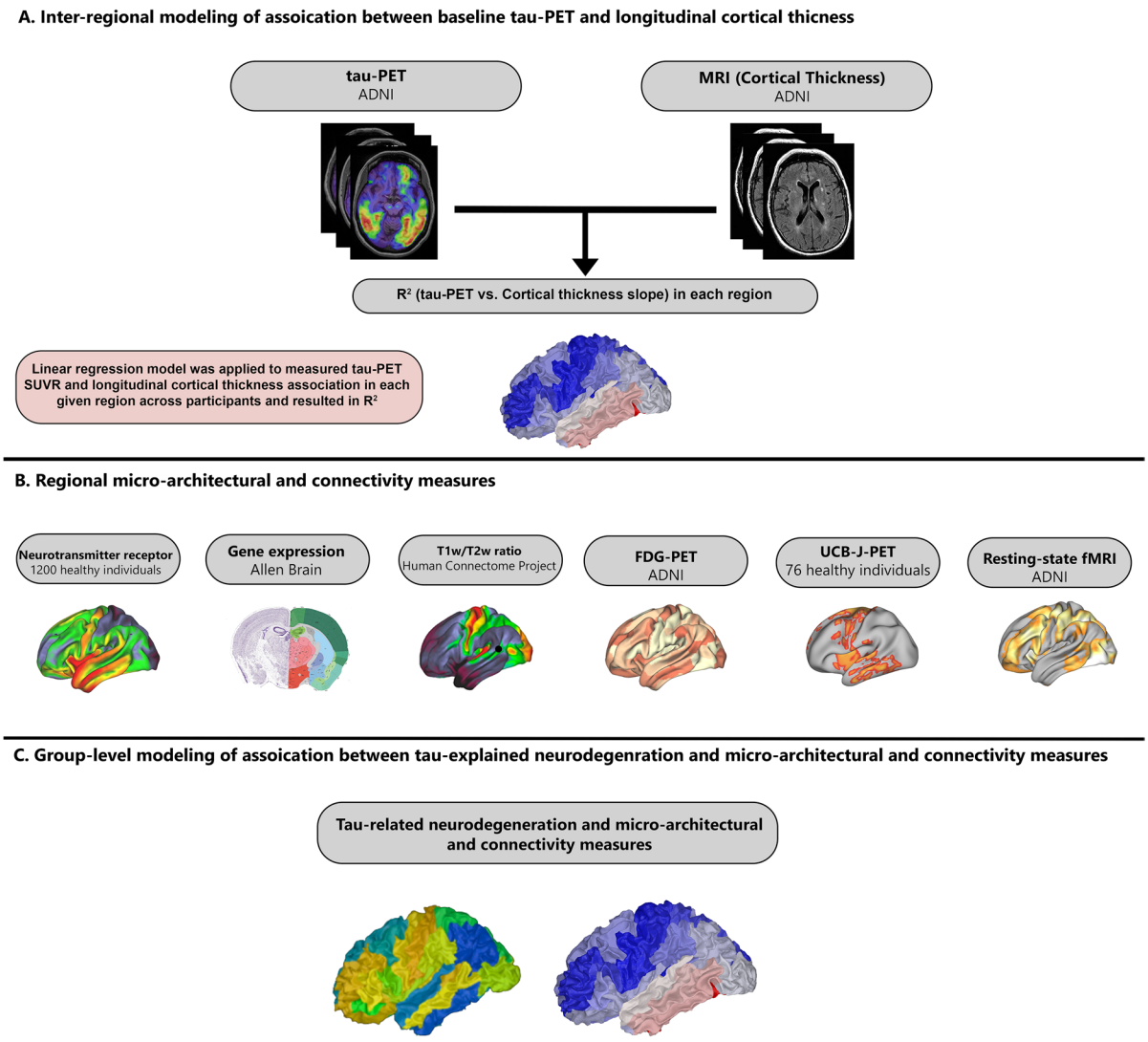

Fig. 1 Methodological approach. Regression analyses of processed baseline tau-PET and longitudinal cortical thickness data in 68 ROIs were performed in order to measure neurodegeneration-explained variance by tau-PET (R^2) in each cortical region (**A**). Regional molecular and connectomic features including 18 PET-derived neurotransmitter receptor densities, 11,560 gene expressions, T1w/T2w ratio (myelination), FDG-PET, UCB-J PET (synaptic density), and rsfMRI were entered as predictors (**B**). See the "Methods" section for details of how the features were retrieved. Spatial similarity between the patterns of tau-explained neurodegeneration (R^2) and molecular and connectomic features was measured using linear regression analyses **C.** ROI, region of interest; PET, positron emission tomography; FDG, 18F-fluorodeoxyglucose; MRI, magnetic resonance imaging; rsfMRI, resting-state functional MRI

Molecular and connectomic features are associated with tau-explained neurodegeneration

My first hypothesis was that molecular and connectomic profiles might affect the association between tau pathology and neurodegeneration. I, therefore, investigated the spatial similarity between the map of calculated R^2 (tau-PET SUVR vs. cortical thickness slope) with molecular and connectivity fingerprints across all participants. I found that the regions with higher E:I ratio and myelination exhibit lower R^2 values (Fig. 6A and D). Also, in the regions where tau explained a low level of variance in cortical atrophy (R^2 value), the synaptic density was significantly

Table 1 Demographic and clinical characteristics

Variable	CU ($n=71$)	MCI ($n=115$)	p
Age (years)	68.1 ± 6.5	74.1 ± 6.1	0.002
Female (%)	42 (59%)	66 (57%)	0.438
Education (years)	16.26 ± 2.6	16.4 ± 2.8	0.633
APOEε4 carriers (%)	21 (26%)	72 (62%)	< 0.001
MMSE	28.2 ± 1.8	26.4 ± 2.4	0.014
CSF total tau (pg/ml)	238.1 ± 67.1	262.4 ± 52.5	0.004
CSF p-tau (pg/ml)	21.6 ± 5.4	24.5 ± 6.8	< 0.001
CSF Aβ (pg/ml)	1373.8 ± 412.4	1123.7 ± 378.2	< 0.001
FDG-PET meta-ROI	1.308 ± 0.612	1.285 ± 0.729	0.0387
Aβ-positive (%)	18 (25%)	62 (54%)	< 0.001

Data are presented as mean ± standard deviation unless specified otherwise

APOEε4 apolipoprotein E genotype (carrying at least one ε4 allele), *MMSE* Mini-Mental State Evaluation, *PET* positron emission tomography, *MCI* mild cognitive impairment, *CU* cognitively healthy, *CSF* cerebrospinal fluid, *p-tau* phosphorylated tau, *FDG-PET* [^{18}F]Fluorodeoxyglucose positron emission tomography

higher (Fig. 6C). Moreover, there was a significant positive association between the glycolytic index and functional connectivity with tau-explained neurodegeneration (R^2 value) (Fig. 6B and E).

Mapping molecular and connectomic profile influence

I inferred to investigate the degree of molecular and connectomic profile influence on tau pathology, neurodegeneration, and tau-explained neurodegeneration (R^2 value) across different brain regions. This was performed by identifying brain regions where the inclusion of a specific molecular and connectomic predictor consistently improved the explanation of a particular type of neuropathology across all subjects. For each molecular and connectomic feature, I fitted individualized, single predictor-enriched models and compared their ability to explain the accumulation of tau pathology, neurodegeneration, or tau-explained neurodegeneration at each brain region. At each brain region, the studentized residuals were computed across all participants, with each residual representing the unexplained pathology (tau pathology, neurodegeneration, or tau-explained neurodegeneration) in a given region. Then, for all regions, the Wilcoxon rank-sum statistics of the population residuals from the two models were calculated. This process was repeated with 1000 randomly shuffled molecular and connectomic maps to obtain a null distribution of Wilcoxon statistics. A permutation test was used to filter brain regions with significant residual improvements ($p<0.05$) over the null distributions. The resulting maps do not represent the regions with the highest pathological severity but rather those were significantly better explained by the inclusion of a particular molecular and connectomic profile distribution. I summarized the molecular and connectomic profile influence map of the factors that were spatial associated with tau pathology, neurodegeneration, or tau-explained neurodegeneration (R^2 value) in the previous steps (Fig. 7).

Among other regions, the glycolytic index most prominently influences tau pathology in right bankssts, fusiform, inferior temporal, pars triangularis, cuneus, entorhinal, pars orbitalis, posterior cingulate, superior temporal, temporal pole, and transverse temporal regions (Fig. 7A). The synaptic density most prominently influences tau pathology in fusiform, inferior parietal, inferior temporal, isthmus cingulate, pars opercularis, bankssts, cuneus, entorhinal, middle temporal, and pars orbitalis regions. The functional connectivity influences tau accumulation in a set of regions including isthmus cingulate, caudal anterior cingulate, rostral anterior cingulate, lateral occipital, lateral orbitofrontal, lingual, superior temporal, bankssts, and caudal middle frontal. Also, the glycolytic index most prominently influences longitudinal alteration of cortical thickness in caudal anterior cingulate, medial orbitofrontal, middle temporal, paracentral, superior temporal, supramarginal, temporal pole, lateral occipital, lateral orbitofrontal, and lingual regions (Fig. 7B). Functional connectivity influences cortical thickness change in entorhinal, lateral orbitofrontal, parahippocampal, postcentral, precentral, posterior cingulate, and superior frontal regions.

In the next step, I repeated the same analysis for the tau-explained neurodegeneration (R^2 value). I found that E:I ratio most prominently influences tau-explained neurodegeneration (R^2 value) in fusiform, inferior parietal, inferior temporal, paracentral, parahippocampal, pars opercularis, bankssts, caudal

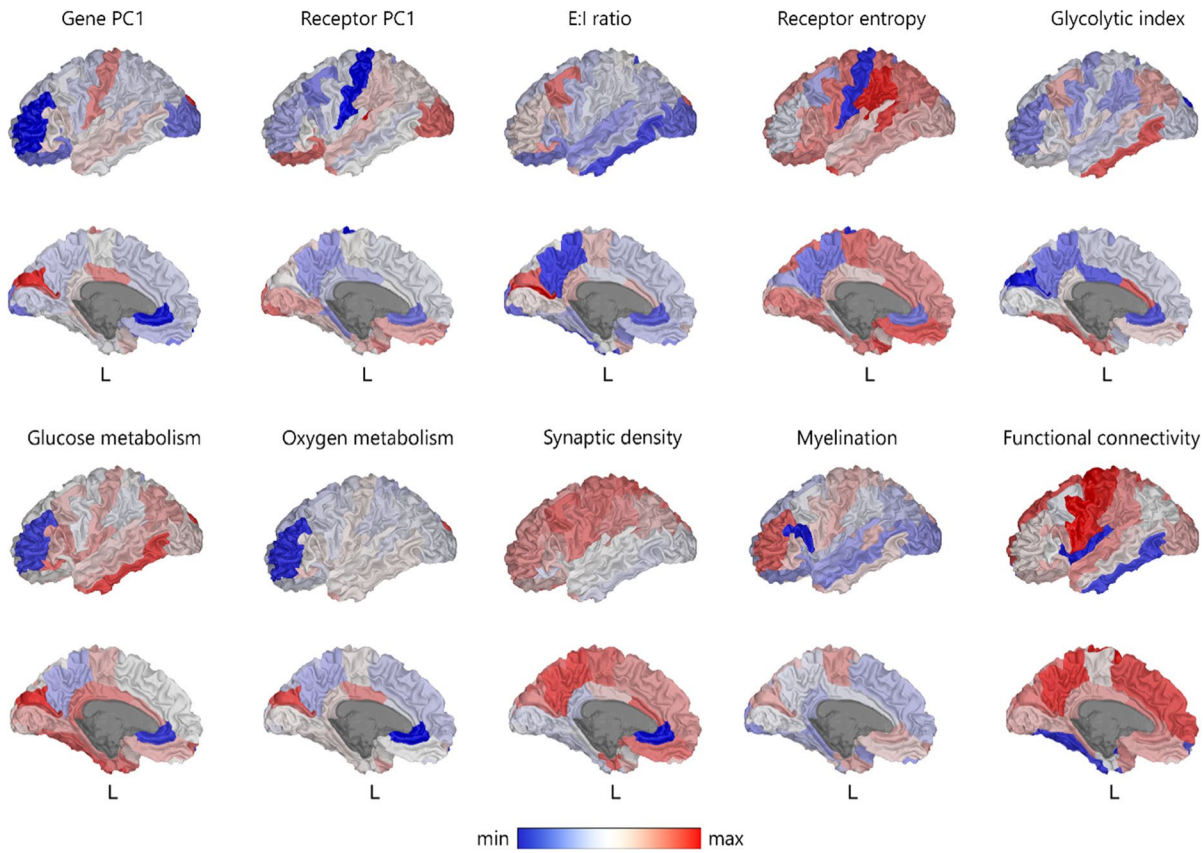

Fig. 2 Microarchitectural and connectomic features. Brain surface rendering of gene PC1 = first component of 11,560 genes' expression, receptor PC1 = first component of 18 PET-derived neurotransmitters density, E:I ratio = excitatory-inhibitory receptor density ratio; receptor entropy, glycolytic index = amount of aerobic glycolysis; glucose metabolism = FDG-PET image; synapse density = UCB-J PET tracer; myelination = T1w/T2w ratio; oxygen metabolism = [^{15}0] labeled water, carbon monoxide, and oxygen PET; functional connectivity = sum of weighted connections. PET, positron emission tomography; FDG, 18F-fluorodeoxyglucose

anterior cingulate, caudal middle frontal, inferior parietal, inferior temporal, insula, and superior temporal regions (Fig. 7C). Also, the glycolytic index influences tau-explained neurodegeneration in fusiform, inferior parietal, pericalcarine, bankssts, caudal anterior cingulate, medial orbitofrontal, middle temporal, and superior frontal regions. Synaptic density influences supramarginal in a set of regions including the frontal pole, fusiform, inferior parietal, parahippocampal, pars opercularis, pars orbitalis, posterior cingulate, superior temporal, and supramarginal. Furthermore, myelination most prominently influences tau-explained neurodegeneration in fusiform, temporal pole, transverse temporal, bankssts, isthmus cingulate, pars opercularis, and superior temporal regions. Functional connectivity influences R^2 value in bankssts, inferior parietal, temporal pole, entorhinal, isthmus cingulate, and parsopercularis regions.

Discussion

The major aim of the current longitudinal study was to assess the molecular and connectivity contributors of tau-related neurodegeneration combining the spatial distribution of molecular and connectomic features and ADNI longitudinal data. Using this patient-specific modeling of longitudinal neuroimaging and normal average spatial template, I found that molecular and connectivity architecture of the human brain is linked to the different effects of tau pathology on neurodegeneration (Fig. 8). Second, I comprehensively

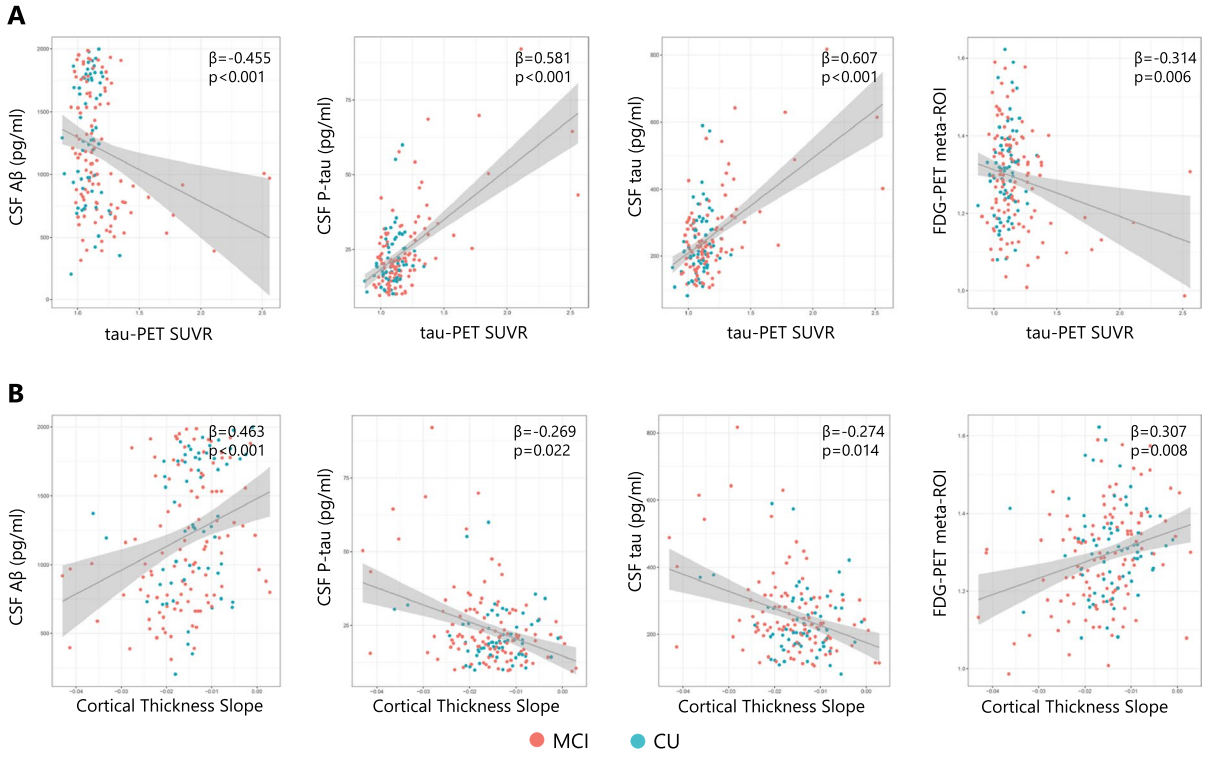

Fig. 3 Association between tau-PET and cortical thickness with CSF biomarkers. Scatter plot of the association between tau-PET SUVR and CSF biomarkers and FDG-PET in meta-ROI regions (**A**). Each dot represents an individual. Scatter plot of the association between cortical thickness slope and CSF biomarkers and FDG-PET in meta-ROI regions (**B**). Each dot represents an individual. All linear regressions performed were two-sided, without adjustment for multiple comparisons, and error bands correspond to the 95% confidence interval. The linear models were adjusted for the effect of age, sex, APOE ε4, and baseline Aβ-PET. PET, positron emission tomography; SUVR, standardized uptake value ratio; Aβ, amyloid-beta; CU, cognitively unimpaired; MCI, mild cognitive impairment; p-tau, phosphorylated tau; FDG-PET, [^{18}F] Fluorodeoxyglucose positron emission tomography

map local molecular and connectivity contributions of tau accumulation and longitudinal neurodegeneration. This study shows that regional vulnerability to tau pathology and neurodegeneration is linked to molecular and connectivity characteristics of the affected brain regions. Third, I further showed that in what regions molecular and connectivity fingerprints most prominently influence the tau pathology, neurodegeneration, and tau-explained neurodegeneration.

Tau aggregates initially accumulate within the medial temporal lobe's memory system, spreading from the transentorhinal cortex to the hippocampus and parahippocampal cortex and eventually extending to other cerebral regions [55–57]. However, the underlying mechanisms determining the selective vulnerability of specific brain regions to tau pathology remain to be clarified. The advance of brain-wide gene expression atlases, such as the Allen Human Brain Atlas, has enabled the correlation of spatial gene expression variations with regional susceptibility to tau pathology in AD [58, 59]. Notably, several studies have identified specific genes whose expression patterns correspond to the spatial distribution of tau pathology [11, 59–61]. Also, brain connectivity is found to be a modifier of tau pathology spreading as regions with stronger connectivity to other regions exhibit higher levels of tau aggregates [47, 62, 63]. It was indicated that pathological tau spreads transsynaptically between neurons in laboratory settings and spreads along axonal connections in the brains of transgenic mouse models of tauopathy. This aligns with the theory of prion-like dissemination of fibrillar tau among interconnected brain regions. In line with previous findings, I found that higher tau pathology

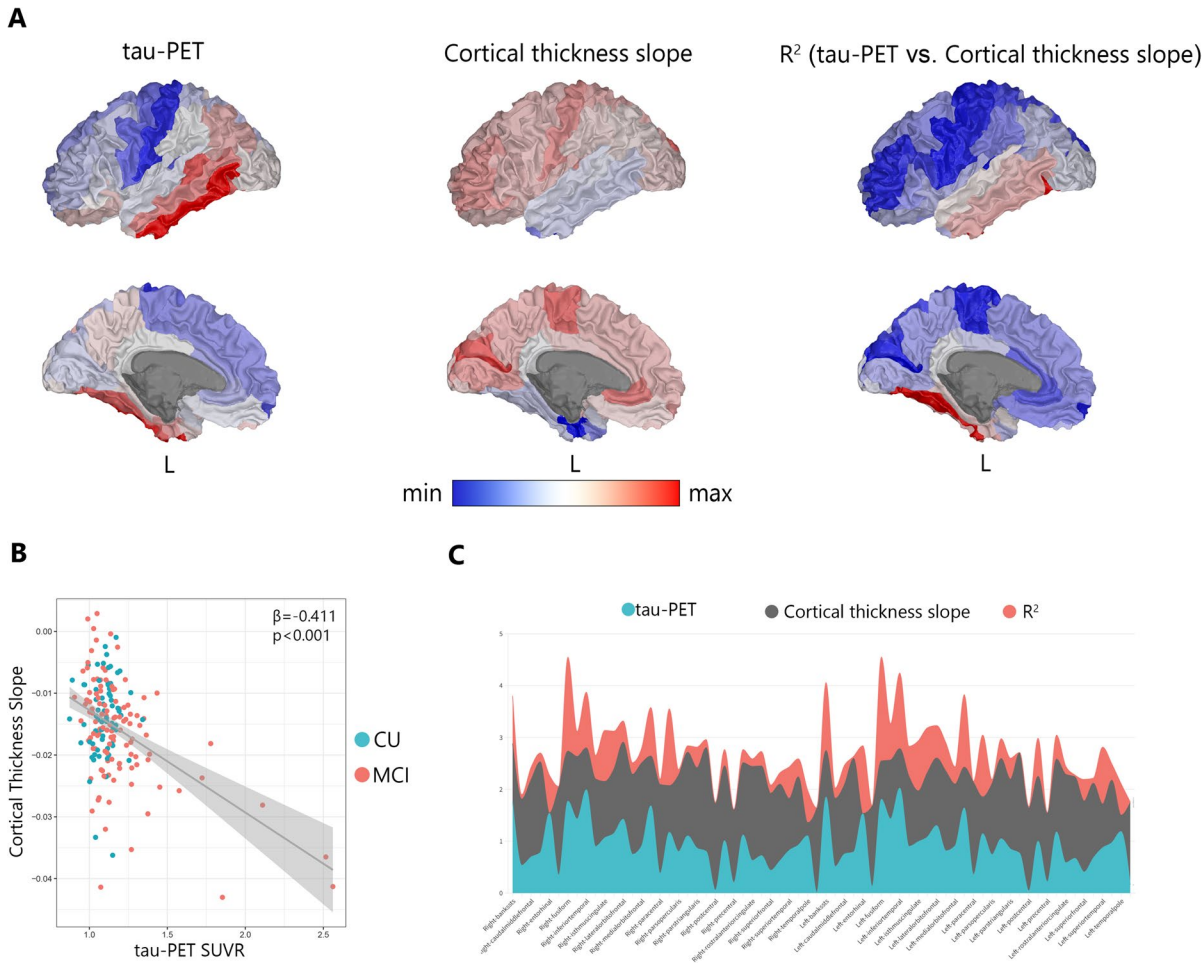

Fig. 4 Regional association between tau-PET and cortical thickness. Surface rendering of average baseline tau-PET, cortical thickness slope, and tau-explained neurodegeneration (R^2) in 68 cortical regions (**A**). Scatter plot of the group-level association between tau-PET SUVR and cortical thickness slope (**B**). Each dot represents an individual. Participants with higher baseline tau-PET SUVR levels have more decrease in cortical thickness over time (**B**). Area chart of regional tau-PET SUVR, cortical thickness slope, and R^2 (tau-PET SUVR vs. cortical thickness slope) (**C**). All linear regressions performed were two-sided, without adjustment for multiple comparisons, and error bands correspond to the 95% confidence interval. The linear models were adjusted for the effect of age, sex, APOE ε4, and baseline Aβ-PET. PET, positron emission tomography; SUVR, standardized uptake value ratio; Aβ, amyloid-beta; CU, cognitively unimpaired; MCI, mild cognitive impairment

is closely linked to the functional connectivity of a given region. Further, I showed that the spatial pattern of tau accumulation is associated with the synaptic density distribution. This finding critically extends previous results, showing an association between baseline tau pathology and longitudinal synaptic loss [64]. Taken together, these findings are congruent with the hypothesis that the local molecular and connectomic characteristics of the brain might play a key role regarding the vulnerability or resilience to tau pathology. Another finding of my study was the slower cortical atrophy over time in regions with higher glycolytic index and functional connectivity. However, my analysis was not adjusted for the effect of tau pathology, which brings the idea that the observed association might be due to the indirect effect of tau pathology since there were similar results for the baseline tau-PET level. However, a previous study demonstrates a significant interplay between tau propagation via communicative connectivity and

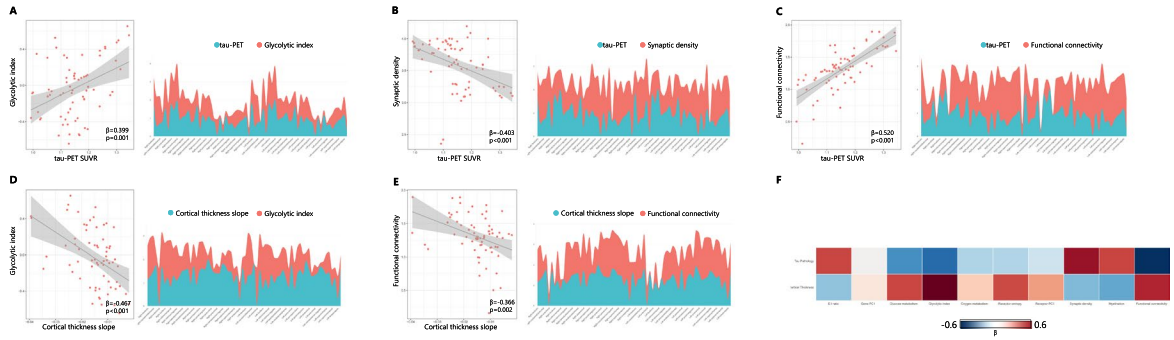

Fig. 5 Microarchitectural and connectomic features are associated with tau pathology and neurodegeneration patterns. Scatter plot and area chart of the association between tau-PET SUVR and glycolytic index (**A**). Each dot represents a region. Regions with higher glycolytic index have higher tau accumulation. Scatter plot and area chart of the association between tau-PET SUVR and synaptic density (**B**). Each dot represents a region. Regions with higher synaptic density showed lower tau accumulation. Scatter plot and area chart of the association between tau-PET SUVR and functional connectivity (**C**). Each dot represents a region. Higher functional connectivity is spatially associated with a higher level of tau accumulation. Scatter plot and area chart of the association between cortical thickness slope and glycolytic index (**D**). Each dot represents a region. A higher glycolytic index is spatially associated with more decrease in cortical thickness over time. Scatter plot and area chart of the association between cortical thickness slope and functional connectivity (**E**). Each dot represents a region. A higher functional connectivity is spatially associated with more decrease in cortical thickness over time. Heatmap of the association between microarchitectural and connectomic features with tau pathology and cortical thickness (**F**). All linear regressions performed were two-sided, without adjustment for multiple comparisons, and error bands correspond to the 95% confidence interval. The linear models were adjusted for the effect of baseline Aβ-PET. PET, positron emission tomography; SUVR, standardized uptake value ratio; Aβ, amyloid-beta

the subsequent impact on glucose metabolism [65]. This underscores the possibility that functional connectivity might partially regulate the effects of tau on FDG metabolism.

Tau pathology is believed to be the main driver of neurodegeneration in the course of AD [56, 66]. Also, previous studies demonstrated a strong spatial and quantitative correlation between tau pathology and neurodegeneration [67, 68]. Nonetheless, both tau and neurodegeneration exhibit variability in their patterns across different brain regions and among individuals, indicating that the relationship between tau and neurodegeneration is not a perfect one-to-one correspondence [69, 70]. To gain a better understanding of early AD pathogenesis, it is important to determine how regional molecular and connectomic features affect the relationship between tau and neurodegeneration. Based on my findings, a higher E:I ratio was spatially associated with a weaker relationship between tau and longitudinal neurodegeneration. The ablation of tau reduces the homeostatic response of the axon initial segments (AISs) in inhibitory neurons, enhances inhibitory activity, and mitigates hypersynchrony. The changes in excitatory and inhibitory neurons elucidate how tau reduction prevents abnormally elevated E:I ratios and subsequent network hypersynchrony and brain disorders [71]. Also, there is more evidence of disrupted excitatory and inhibitory synaptic functions linked to tau in early AD [72]. Pathological tau accumulation occurs predominantly in excitatory neurons as opposed to inhibitory neurons [73]. This pattern is observed in the entorhinal cortex, along with brain regions affected in the later stages of the disease [73]. In combination with my findings, regions with higher excitatory synaptic function are less vulnerable to tau-related neurodegeneration which offers the therapeutic potential of neurotransmitter-based treatments in the AD continuum.

Elevated myelin levels are associated with a reduced susceptibility of the connected regions to tau aggregate accumulation [74]. Further, defects in myelin lipid biosynthesis at the preclinical stages of AD precede tau pathology in cortical regions [75]. I showed that the regions with higher template-based myelination have lower tau-explained neurodegeneration. These results suggest that the myelination might have a protective role in the downstream

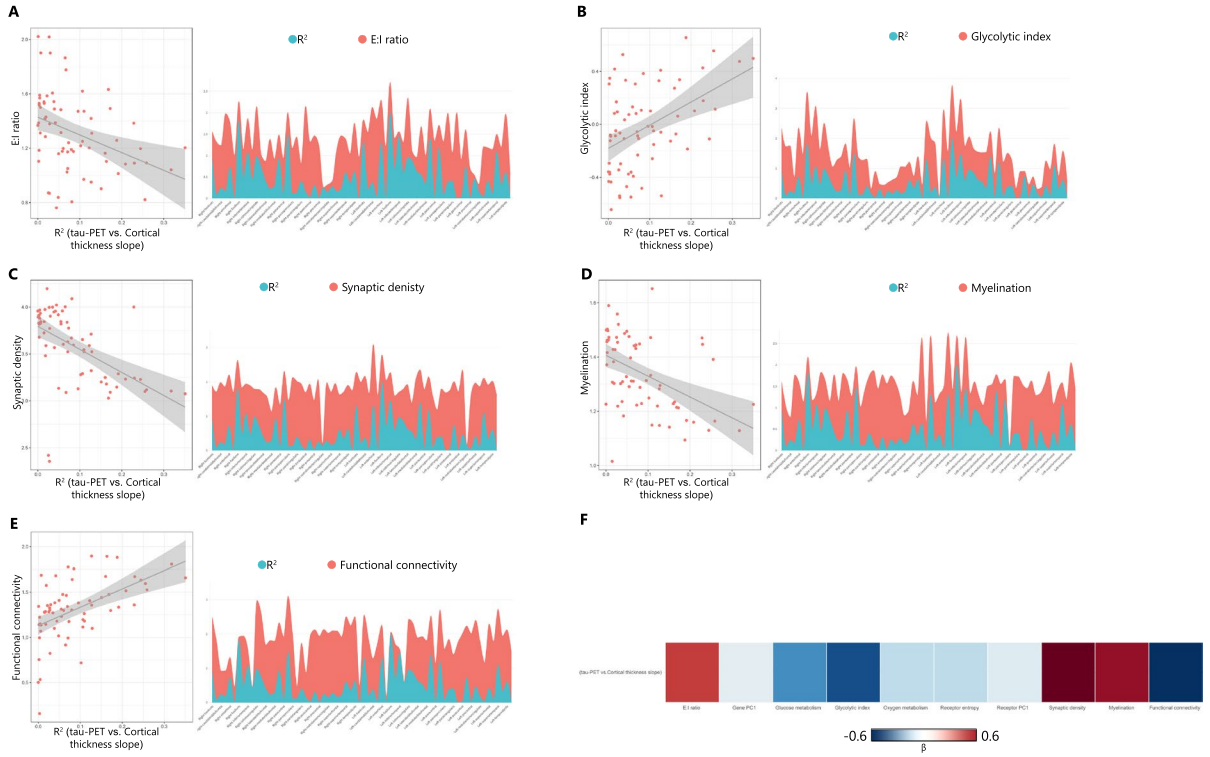

Fig. 6 Microarchitectural and connectomic features are associated with tau-explained neurodegeneration. Scatter plot and area chart of the association between tau-explained neurodegeneration (R^2) and E:I ratio (**A**). Each dot represents a region. Regions with higher E:I have lower tau-explained neurodegeneration (R^2). Scatter plot and area chart of the association between tau-explained neurodegeneration (R^2) and glycolytic index (**B**). Each dot represents a region. Regions with higher glycolytic index have higher tau-explained neurodegeneration (R^2). Scatter plot and area chart of the association between tau-explained neurodegeneration (R^2) and synaptic density (**C**). Each dot represents a region. Regions with higher synaptic density have lower tau-explained neurodegeneration (R^2). Scatter plot and area chart of the association between tau-explained neurodegeneration (R^2) and myelination (**D**). Each dot represents a region. Regions with higher myelination have lower tau-explained neurodegeneration (R^2). Scatter plot and area chart of the association between tau-explained neurodegeneration (R^2) and functional connectivity (**E**). Each dot represents a region. Regions with higher functional connectivity have higher tau-explained neurodegeneration (R^2). Heatmap of the association between microarchitectural and connectomic features with tau-explained neurodegeneration (R^2) (**F**). All linear regressions performed were two-sided, without adjustment for multiple comparisons, and error bands correspond to the 95% confidence interval. The linear models were adjusted for the effect of baseline Aβ-PET. PET, positron emission tomography; Aβ, amyloid-beta; E:I ratio, excitatory: inhibitory receptor density ratio

neurodegeneration due to the tau pathology. The current findings suggest that myelin may serve as a potential target for the prevention and treatment of AD. Given that myelination is a druggable target, pharmacological stimulation of myelination emerges as a promising therapeutic strategy for AD [76, 77]. Clemastine, an approved H1 histamine antagonist, has recently been demonstrated to enhance the differentiation of oligodendrocyte precursor cells and promote myelination [78]. Clinical trials repurposing clemastine for the treatment of multiple sclerosis have shown symptom improvement [79].

Synapses play a critical role in cognitive function, and synaptic loss is a well-documented and consistent pathology in AD [80]. Cognitive impairment in AD is strongly correlated with synaptic loss in the association cortex and limbic system [81]. Synaptic damage linked to toxic β-amyloid oligomers and tau aggregates is evident in the early clinical stages of AD, with individuals with mild

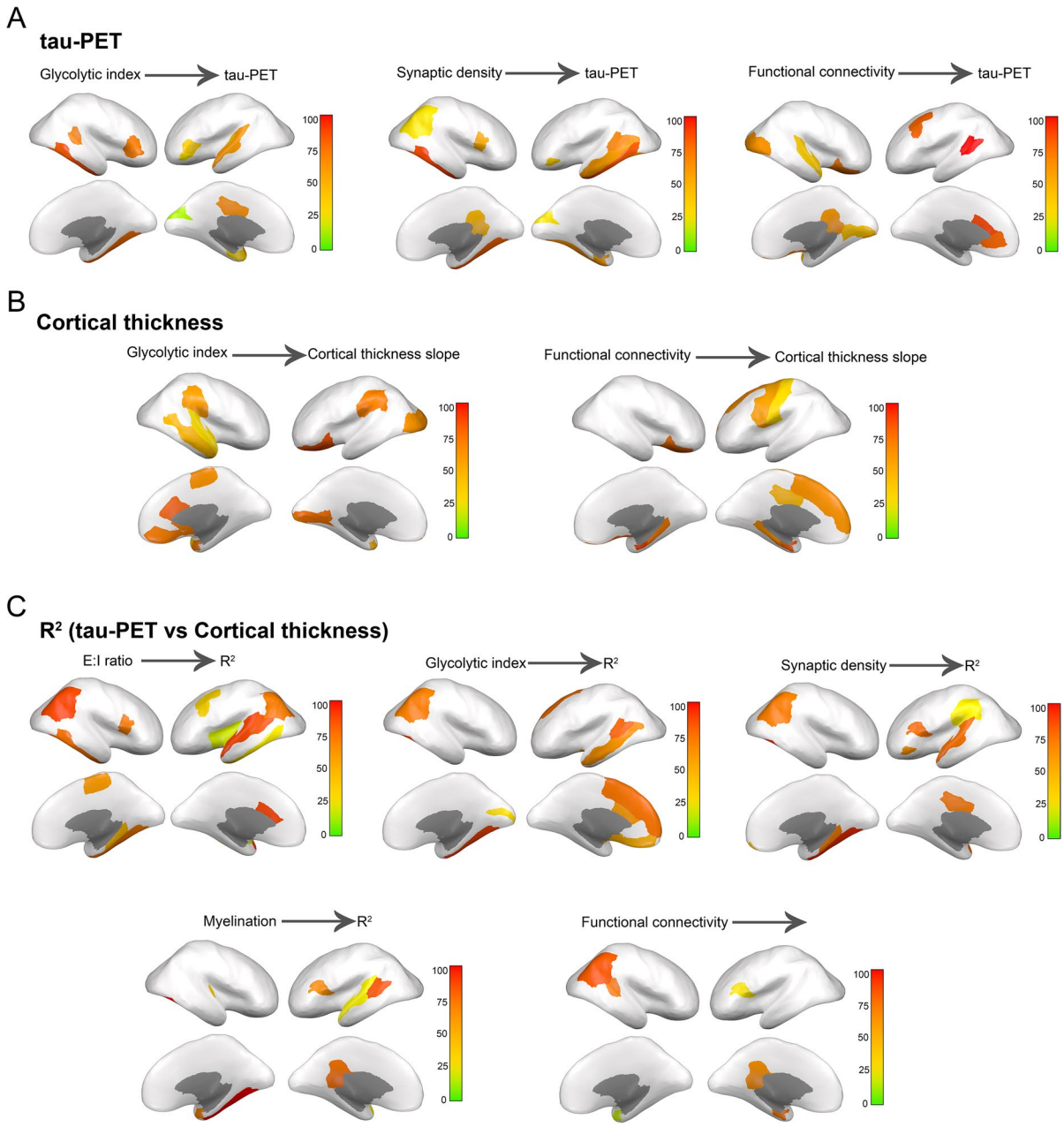

Fig. 7 Model-derived map of molecular and connectomic influence on tau pathology, neurodegeneration, and tau-explained neurodegeneration. The influence map of molecular and connectomic features visualized on the brain (**A**–**C**). The influence map shows the brain regions where specific molecular and connectomic features are consistently informative in explaining the tau pathology, neurodegeneration (cortical thickness derived from MRI data), or tau-explained neurodegeneration which were re-scaled to 0 to 100 range for visualization. It shows the change in model residuals at each region due to adding the molecular and connectomic profile as a model predictor of tau pathology, neurodegeneration, or tau-explained neurodegeneration. The receptor influences are calculated using the Wilcoxon rank-sum test statistics of the residuals from each model for a given region. The maps presented show only the regions with statistically significant z-scores (p-value < 0.05) of the Wilcoxon rank-sum test statistics, relative to the null distributions

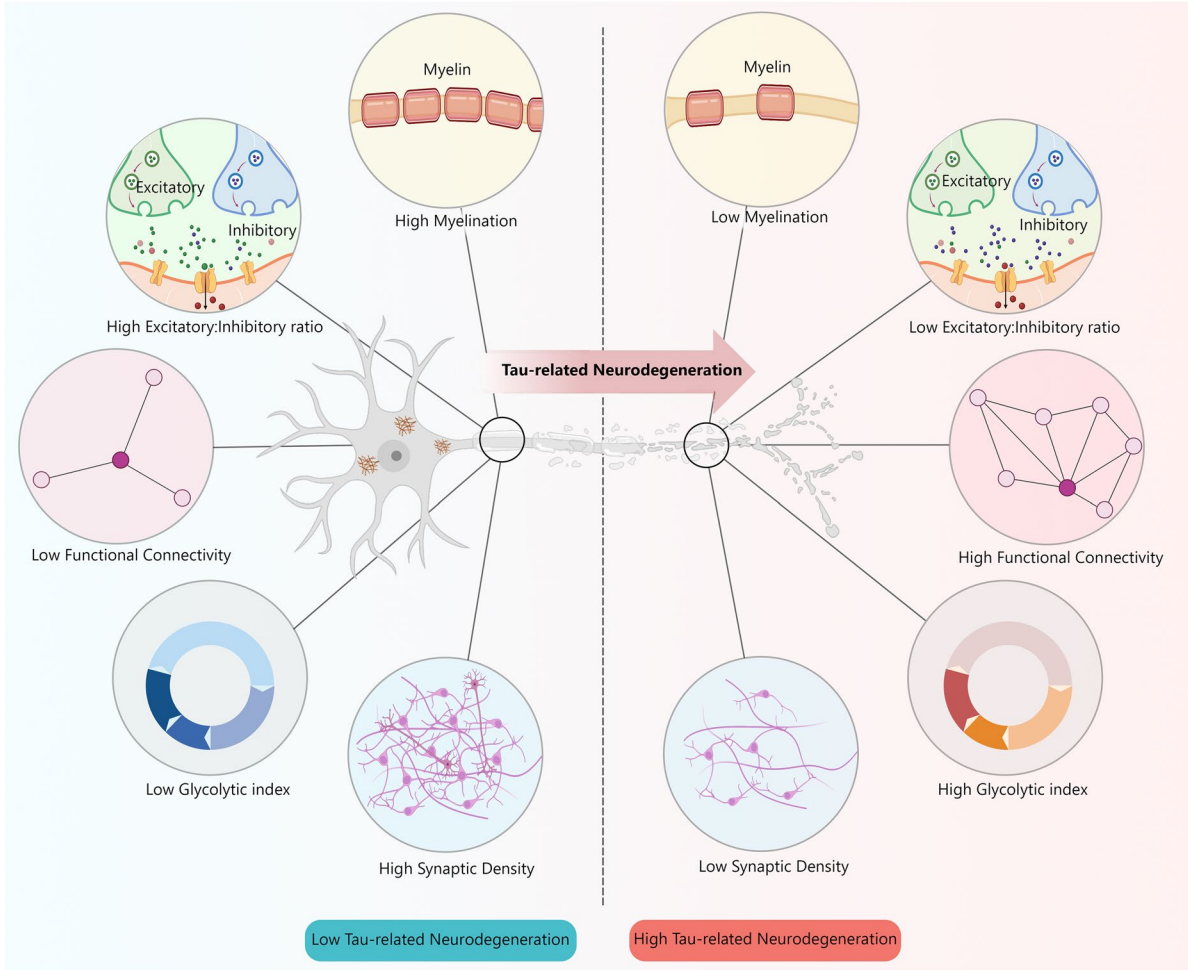

Fig. 8 Proposed model of microarchitectural and connectomic features associated with tau-related neurodegeneration. The model revealed that biological and connectomic profiles including lower myelination, excitatory-inhibitory receptor density ratio, and synaptic density along with higher functional connectivity and glycolytic index are associated with the pattern of higher neurodegeneration due to the tau pathology

MCI exhibiting a reduction in synapses and synaptic density [82]. Post-mortem studies suggest that pathological tau impairs synaptic function through several mechanisms, including interference with presynaptic vesicle release and the translocation of tau toward dendrites in the postsynapse, which is associated with dendritic loss [83]. An in vivo study revealed that loss of synaptic density regionally follows tau accumulation after 2 years [84]. Based on my findings, regions with high synaptic density are less vulnerable to neurodegeneration due to the tau pathology.

Another important finding of the present study was the higher tau-related neurodegeneration in regions with stronger connectivity to other regions. A possible explanation might be the trans-synaptic spread of tau aggregates through functional connections and the local effect of tau pathology on the synapses [47, 85]. A study by Wang et al. suggested that functional connectivity partially modulates the influence of tau accumulation on downstream glucose metabolism [65].

Previous studies support the notion that a deviation from the normative relationship between tau

pathology and neurodegeneration across brain regions in the AD continuum might be due to multiple non-AD underlying factors [4, 10, 17]. However, this is the first study aimed to explore the regional molecular and connectivity fingerprints affecting the relationship between tau pathology and downstream neurodegeneration. The strength of this study is the integration of longitudinal data to investigate neurodegeneration, facilitating a dynamic and temporal understanding of disease progression. By concentrating on the regional molecular and connectivity fingerprints that modulate the relationship between tau pathology and subsequent neurodegeneration, the study provides a deep understanding of the mechanisms underlying AD neurodegeneration.

This data-driven methodology requires validation through post-mortem pathological analysis to ascertain whether the resilience or vulnerability imaging patterns are accurately captured. Despite this necessity, the approach holds significant implications for clinical interventions and prognostication, especially as a proxy for neurodegenerative disorders lacking in vivo biomarkers. Also, investigating the tau and neurodegeneration mismatch could also facilitate the identification and examination of resilience or brain reserve. If corroborated with longitudinal cognitive data, it may serve as a valuable prognostic instrument for clinicians.

There are also several limitations to consider. Firstly, using longitudinal tau-PET imaging would better capture the tau aggregate accumulation in the early stages of AD. Second, neuropathological validation is crucial for this study. However, there is a lack of access to datasets that include tau-PET, 18F-FDG-PET, and autopsy data. Third, although I used linear regression to determine the relationship between tau pathology and neurodegeneration, the relationship is likely to exhibit some degree of nonlinearity. Nonlinear approaches, such as image-to-image translation, may more accurately model the relationships, including potential remote spatial dependencies between network hubs and connected nodes. Another limitation is the exclusion of AD patients during the selection phase, due to their limited number. Consequently, the study is unable to elucidate the impact of Aβ plaques on tau propagation. Additionally, the tau pathology burden among the CU and MCI participants within the ADNI dataset is relatively low. This results in a low signal-to-noise ratio for tau-PET imaging, particularly at the lower end of the spectrum, which may lead to the measurement of scan noise rather than a clear signal of tau pathology.

The current study demonstrates that the regional susceptibility to tau-related neurodegeneration is associated with specific molecular and connectomic characteristics of the affected neural systems. I found that the molecular and connectivity architecture of the human brain is linked to the different effects of tau pathology on downstream neurodegeneration. This may improve our understanding regarding the potential factors that shape cortical neurodegeneration due to the tau pathology which paves the way for a step toward the implementation of precision medicine in AD. However, future studies will need to apply this approach with a larger sample size; personalized molecular and connectomic characteristics, incorporating directional flow; and Aβ dynamics.

Acknowledgements Data collection and sharing for this project were provided by the Alzheimer's Disease Neuroimaging Initiative (ADNI) (National Institutes of Health Grant U01 AG024904) and DOD ADNI (Department of Defense award number W81XWH-12-2-0012). ADNI is funded by the National Institute on Aging, the National Institute of Biomedical Imaging and Bioengineering, and through generous contributions from the following: AbbVie, Alzheimer's Association; Alzheimer's Drug Discovery Foundation; Araclon Biotech; BioClinica, Inc.; Biogen; Bristol-Myers Squibb Company; CereSpir, Inc.; Cogstate; Eisai Inc.; Elan Pharmaceuticals, Inc.; Eli Lilly and Company; EuroImmun; F. Hoffmann-La Roche Ltd. and its affiliated company Genentech, Inc.; Fujirebio; GE Healthcare; IXICO Ltd.; Janssen Alzheimer Immunotherapy Research & Development, LLC.; Johnson & Johnson Pharmaceutical Research & Development LLC.; Lumosity; Lundbeck; Merck & Co., Inc.; Meso Scale Diagnostics, LLC.; NeuroRx Research; Neurotrack Technologies; Novartis Pharmaceuticals Corporation; Pfizer Inc.; Piramal Imaging; Servier; Takeda Pharmaceutical Company; and Transition Therapeutics. The Canadian Institutes of Health Research is providing funds to support ADNI clinical sites in Canada. Private sector contributions are facilitated by the Foundation for the National Institutes of Health (www.fnih.org). The grantee organization is the Northern California Institute for Research and Education, and the study is coordinated by the Alzheimer's Therapeutic Research Institute at the University of Southern California. ADNI data are disseminated by the Laboratory for Neuro Imaging at the University of Southern California.

Consortia

Alzheimer's Disease Neuroimaging Initiative

Michael W. Weiner, Paul Aisen, Ronald Petersen, Clifford R. Jack, William Jagust, John Q. Trojanowski, Arthur W. Toga, Laurel Beckett, Robert C. Green, Andrew J. Saykin, John Morris, Leslie M. Shaw, Zaven Khachaturian, Greg Sorensen, Lew Kuller, Marcus Raichle, Steven Paul, Peter Davies, Howard Fillit, Franz Hefti, David Holtzman, Marek M. Mesulam, William

Potter, Peter Snyder, Adam Schwartz, Tom Montine, Ronald G. Thomas, Michael Donohue, Sarah Walter, Devon Gessert, Tamie Sather, Gus Jiminez, Danielle Harvey, Matthew Bernstein, Paul Thompson, Norbert Schuff, Bret Borowski, Jeff Gunter, Matt Senjem, Prashanthi Vemuri, David Jones, Kejal Kantarci, Chad Ward, Robert A. Koeppe, Norm Foster, Eric M. Reiman, Kewei Chen, Chet Mathis, Susan Landau, Nigel J. Cairns, Erin Householder, Lisa Taylor-Reinwald, Virginia Lee, Magdalena Korecka, Michal Figurski, Karen Crawford, Scott Neu, Tatiana M. Foroud, Steven G. Potkin, Li Shen, Kelley Faber, Sungeun Kim, Kwangsik Nho, Leon Thal, Neil Buckholtz, Marylyn Albert, Richard Frank, John Hsiao, Jeffrey Kaye, Joseph Quinn, Betty Lind, Raina Carter, Sara Dolen, Lon S. Schneider, Sonia Pawluczyk, Mauricio Beccera, Liberty Teodoro, Bryan M. Spann, James Brewer, Helen Vanderswag, Adam Fleisher, Judith L. Heidebrink, Joanne L. Lord, Sara S. Mason, Colleen S. Albers, David Knopman, Kris Johnson, Rachelle S. Doody, Javier Villanueva-Meyer, Munir Chowdhury, Susan Rountree, Mimi Dang, Yaakov Stern, Lawrence S. Honig, Karen L. Bell, Beau Ances, Maria Carroll, Sue Leon, Mark A. Mintun, Stacy Schneider, Angela Oliver, Daniel Marson, Randall Griffith, David Clark, David Geldmacher, John Brockington, Erik Roberson, Hillel Grossman, Effie Mitsis, Leyla de Toledo-Morrell, Raj C. Shah, Ranjan Duara, Daniel Varon, Maria T. Greig, Peggy Roberts, Chiadi Onyike, Daniel D'Agostino, Stephanie Kielb, James E. Galvin, Brittany Cerbone, Christina A. Michel, Henry Rusinek, Mony J. de Leon, Lidia Glodzik, Susan De Santi, PMurali Doraiswamy, Jeffrey R. Petrella, Terence Z. Wong, Steven E. Arnold, Jason H. Karlawish, David Wolk, Charles D. Smith, Greg Jicha, Peter Hardy, Partha Sinha, Elizabeth Oates, Gary Conrad, Oscar L. Lopez, MaryAnn Oakley, Donna M. Simpson, Anton P. Porsteinsson, Bonnie S. Goldstein, Kim Martin, Kelly M. Makino, MSaleem Ismail, Connie Brand, Ruth A. Mulnard, Gaby Thai, Catherine McAdams-Ortiz, Kyle Womack, Dana Mathews, Mary Quiceno, Ramon Diaz-Arrastia, Richard King, Myron Weiner, Kristen Martin-Cook, Michael DeVous, Allan I. Levey, James J. Lah, Janet S. Cellar, Jeffrey M. Burns, Heather S. Anderson, Russell H. Swerdlow, Liana Apostolova, Kathleen Tingus, Ellen Woo, Daniel H. S. Silverman, Po H. Lu, George Bartzokis, Neill R. Graff-Radford, Francine Parfitt, Tracy Kendall, Heather Johnson, Martin R. Farlow, Ann Marie Hake, Brandy R. Matthews, Scott Herring, Cynthia Hunt, Christopher H. van Dyck, Richard E. Carson, Martha G. MacAvoy, Howard Chertkow, Howard Bergman, Chris Hosein, Ging-Yuek Robin Hsiung, Howard Feldman, Benita Mudge, Michele Assaly, Charles Bernick, Donna Munic, Andrew Kertesz, John Rogers, Dick Trost, Diana Kerwin, Kristine Lipowski, Chuang-Kuo Wu, Nancy Johnson, Carl Sadowsky, Walter Martinez, Teresa Villena, Raymond Scott Turner, Kathleen Johnson, Brigid Reynolds, Reisa A. Sperling, Keith A. Johnson, Gad Marshall, Meghan Frey, Barton Lane, Allyson Rosen, Jared Tinklenberg, Marwan N. Sabbagh, Christine M. Belden, Sandra A. Jacobson, Sherye A. Sirrel, Neil Kowall, Ronald Killiany, Andrew E. Budson, Alexander Norbash, Patricia Lynn Johnson, Joanne Allard, Alan Lerner, Paula Ogrocki, Leon Hudson, Evan Fletcher, Owen Carmichae, John Olichney, Charles DeCarli, Smita Kittur, Michael Borrie, T.-Y. Lee, Rob Bartha, Sterling Johnson, Sanjay Asthana, Cynthia M. Carlsson, Adrian Preda, Dana Nguyen, Pierre Tariot, Stephanie Reeder, Vernice Bates, Horacio Capote, Michelle Rainka, Douglas W. Scharre, Maria Kataki, Anahita Adeli, Earl A. Zimmerman, Dzintra Celmins, Alice D. Brown, Godfrey D. Pearlson, Karen Blank, Karen Anderson, Robert B. Santulli, Tamar J. Kitzmiller, Eben S. Schwartz, Kaycee M. Sink, Jeff D. Williamson, Pradeep Garg, Franklin Watkins, Brian R. Ott, Henry Querfurth, Geoffrey Tremont, Stephen Salloway, Paul Malloy, Stephen Correia, Howard J. Rosen, Bruce L. Miller, Jacobo Mintzer, Kenneth Spicer, David Bachman, Stephen Pasternak, Irina Rachinsky, Dick Drost, Nunzio Pomara, Raymundo Hernando, Antero Sarrael, Susan K. Schultz, Laura L. Boles Ponto, Hyungsub Shim, Karen Elizabeth Smith, Norman Relkin, Gloria Chaing, Lisa Raudin, Amanda Smith, Kristin Fargher, Balebail Ashok Raj, Thomas Neylan, Jordan Grafman, Melissa Davis, Rosemary Morrison, Jacqueline Hayes, Shannon Finley, Karl Friedl, Debra Fleischman, Konstantinos Arfanakis, Olga James, Dino Massoglia, JJay Fruehling, Sandra Harding, Elaine R. Peskind, Eric C. Petrie, Gail Li, Jerome A. Yesavage, Joy L. Taylor, and Ansgar J. Furst.

Author contribution Data collecting, analysis, supervision, concept, and drafting were done by Fardin Nabizadeh.

Data availability The datasets generated and/or analyzed during the current study are available in the ADNI repository, https://adni.loni.usc.edu/. Neurotransmitter receptor data is available at https://github.com/netneurolab/hansen_crossdisorder_vulnerability. The datasets used and/or analyzed during the current study are available from the corresponding author upon reasonable request.

Declarations

Ethical approval The protocol for the research project has been approved by a suitably constituted Ethics Committee of an institution, and it conforms to the provisions of the Declaration of Helsinki according to the ADNI study (adni.loni.usc.edu). The STROBE checklist was followed in this observational study.

Consent for publication This manuscript has been approved for publication by all authors.

Conflict of interest The author declares no competing interests.

References

1. Jack CR Jr, Bennett DA, Blennow K, Carrillo MC, Dunn B, Haeberlein SB, et al. NIA-AA Research Framework: Toward a biological definition of Alzheimer's disease. Alzheimers Dement. 2018;14(4):535–62.
2. Selkoe DJ, Hardy J. The amyloid hypothesis of Alzheimer's disease at 25 years. EMBO Mol Med. 2016;8(6):595–608.

3. Scheltens P, De Strooper B, Kivipelto M, Holstege H, Chételat G, Teunissen CE, et al. Alzheimer's disease. The Lancet. 2021;397(10284):1577–90.
4. Das SR, Lyu X, Duong MT, Xie L, McCollum L, de Flores R, et al. Tau-atrophy variability reveals phenotypic heterogeneity in Alzheimer's disease. Ann Neurol. 2021;90(5):751–62.
5. Guo T, Zhang D, Zeng Y, Huang TY, Xu H, Zhao Y. Molecular and cellular mechanisms underlying the pathogenesis of Alzheimer's disease. Mol Neurodegener. 2020;15(1):40.
6. Knopman DS, Lundt ES, Therneau TM, Vemuri P, Lowe VJ, Kantarci K, et al. Entorhinal cortex tau, amyloid-β, cortical thickness and memory performance in non-demented subjects. Brain. 2019;142(4):1148–60.
7. Schöll M, Lockhart SN, Schonhaut DR, O'Neil JP, Janabi M, Ossenkoppele R, et al. PET imaging of Tau deposition in the aging human brain. Neuron. 2016;89(5):971–82.
8. Das SR, Xie L, Wisse LEM, Ittyerah R, Tustison NJ, Dickerson BC, et al. Longitudinal and cross-sectional structural magnetic resonance imaging correlates of AV-1451 uptake. Neurobiol Aging. 2018;66:49–58.
9. Otero-Garcia M, Mahajani SU, Wakhloo D, Tang W, Xue YQ, Morabito S, et al. Molecular signatures underlying neurofibrillary tangle susceptibility in Alzheimer's disease. Neuron. 2022;110(18):2929-48.e8.
10. Lyu X, Duong MT, Xie L, de Flores R, Richardson H, Hwang G, et al. Tau-neurodegeneration mismatch reveals vulnerability and resilience to comorbidities in Alzheimer's continuum. Alzheimers Dement. 2024;20(3):1586–600.
11. Zheng L, Rubinski A, Denecke J, Luan Y, Smith R, Strandberg O, et al. Combined connectomics, MAPT gene expression, and amyloid deposition to explain regional tau deposition in Alzheimer disease. Ann Neurol. 2024;95(2):274–87.
12. Tracy TE, Madero-Pérez J, Swaney DL, Chang TS, Moritz M, Konrad C, et al. Tau interactome maps synaptic and mitochondrial processes associated with neurodegeneration. Cell. 2022;185(4):712-28.e14.
13. Zhang X, Alshakhshir N, Zhao L. Glycolytic metabolism, brain resilience, and Alzheimer's disease. Front Neurosci. 2021;15:662242.
14. Latimer CS, Burke BT, Liachko NF, Currey HN, Kilgore MD, Gibbons LE, et al. Resistance and resilience to Alzheimer's disease pathology are associated with reduced cortical pTau and absence of limbic-predominant age-related TDP-43 encephalopathy in a community-based cohort. Acta Neuropathol Commun. 2019;7(1):91.
15. Zalocusky KA, Najm R, Taubes AL, Hao Y, Yoon SY, Koutsodendris N, et al. Neuronal ApoE upregulates MHC-I expression to drive selective neurodegeneration in Alzheimer's disease. Nat Neurosci. 2021;24(6):786–98.
16. Shi Y, Andhey PS, Ising C, Wang K, Snipes LL, Boyer K, et al. Overexpressing low-density lipoprotein receptor reduces tau-associated neurodegeneration in relation to apoE-linked mechanisms. Neuron. 2021;109(15):2413-26.e7.
17. Duong MT, Das SR, Lyu X, Xie L, Richardson H, Xie SX, et al. Dissociation of tau pathology and neuronal hypometabolism within the ATN framework of Alzheimer's disease. Nat Commun. 2022;13(1):1495.
18. Khan AF, Adewale Q, Baumeister TR, Carbonell F, Zilles K, Palomero-Gallagher N, et al. Personalized brain models identify neurotransmitter receptor changes in Alzheimer's disease. Brain. 2022;145(5):1785–804.
19. Negro D, Opazo P (2024) Cognitive resilience in Alzheimer's disease: from large-scale brain networks to synapses. Brain Commun 6(1). https://doi.org/10.1093/braincomms/fcae050
20. Buckner RL, Sepulcre J, Talukdar T, Krienen FM, Liu H, Hedden T, et al. Cortical hubs revealed by intrinsic functional connectivity: mapping, assessment of stability, and relation to Alzheimer's disease. J Neurosci. 2009;29(6):1860–73.
21. Landau S, Jagust W (2016) Flortaucipir (AV-1451) processing methods. Alzheimer's Disease Neuroimaging Initiative
22. Jack CR Jr, Bernstein MA, Fox NC, Thompson P, Alexander G, Harvey D, et al. The Alzheimer's disease neuroimaging initiative (ADNI): MRI methods. J Magn Reson Imaging. 2008;27(4):685–91.
23. Fischl B, Salat DH, van der Kouwe AJ, Makris N, Ségonne F, Quinn BT, et al. Sequence-independent segmentation of magnetic resonance images. Neuroimage. 2004;23(Suppl 1):S69-84.
24. Hawrylycz MJ, Lein ES, Guillozet-Bongaarts AL, Shen EH, Ng L, Miller JA, et al. An anatomically comprehensive atlas of the adult human brain transcriptome. Nature. 2012;489(7416):391–9.
25. Hansen JY, Markello RD, Vogel JW, Seidlitz J, Bzdok D, Misic B. Mapping gene transcription and neurocognition across human neocortex. Nat Hum Behav. 2021;5(9):1240–50.
26. Hawrylycz M, Miller JA, Menon V, Feng D, Dolbeare T, Guillozet-Bongaarts AL, et al. Canonical genetic signatures of the adult human brain. Nat Neurosci. 2015;18(12):1832–44.
27. Hansen JY, Shafiei G, Markello RD, Smart K, Cox SML, Nørgaard M, et al. Mapping neurotransmitter systems to the structural and functional organization of the human neocortex. Nat Neurosci. 2022;25(11):1569–81.
28. Vaishnavi SN, Vlassenko AG, Rundle MM, Snyder AZ, Mintun MA, Raichle ME. Regional aerobic glycolysis in the human brain. Proc Natl Acad Sci U S A. 2010;107(41):17757–62.
29. Finnema SJ, Nabulsi NB, Mercier J, Lin SF, Chen MK, Matuskey D, et al. Kinetic evaluation and test-retest reproducibility of [(11)C]UCB-J, a novel radioligand for positron emission tomography imaging of synaptic vesicle glycoprotein 2A in humans. J Cereb Blood Flow Metab. 2018;38(11):2041–52.
30. Chen MK, Mecca AP, Naganawa M, Gallezot JD, Toyonaga T, Mondal J, et al. Comparison of [(11)C]UCB-J and [(18)F]FDG PET in Alzheimer's disease: a tracer kinetic modeling study. J Cereb Blood Flow Metab. 2021;41(9):2395–409.
31. O'Dell RS, Mecca AP, Chen MK, Naganawa M, Toyonaga T, Lu Y, et al. Association of Aβ deposition and regional synaptic density in early Alzheimer's disease: a

PET imaging study with [(11)C]UCB-J. Alzheimers Res Ther. 2021;13(1):11.
32. Smart K, Liu H, Matuskey D, Chen MK, Torres K, Nabulsi N, et al. Binding of the synaptic vesicle radiotracer [(11)C]UCB-J is unchanged during functional brain activation using a visual stimulation task. J Cereb Blood Flow Metab. 2021;41(5):1067–79.
33. Weiss JJ, Calvi R, Naganawa M, Toyonaga T, Farhadian SF, Chintanaphol M, et al. Preliminary in vivo evidence of reduced synaptic density in human immunodeficiency virus (HIV) despite Antiretroviral therapy. Clin Infect Dis. 2021;73(8):1404–11.
34. Radhakrishnan R, Skosnik PD, Ranganathan M, Naganawa M, Toyonaga T, Finnema S, et al. In vivo evidence of lower synaptic vesicle density in schizophrenia. Mol Psychiatry. 2021;26(12):7690–8.
35. Finnema SJ, Toyonaga T, Detyniecki K, Chen MK, Dias M, Wang Q, et al. Reduced synaptic vesicle protein 2A binding in temporal lobe epilepsy: a [(11) C] UCB-J positron emission tomography study. Epilepsia. 2020;61(10):2183–93.
36. Bini J, Holden D, Fontaine K, Mulnix T, Lu Y, Matuskey D, et al. Human adult and adolescent biodistribution and dosimetry of the synaptic vesicle glycoprotein 2A radioligand (11)C-UCB-J. EJNMMI Res. 2020;10(1):83.
37. Mecca AP, Chen MK, O'Dell RS, Naganawa M, Toyonaga T, Godek TA, et al. In vivo measurement of widespread synaptic loss in Alzheimer's disease with SV2A PET. Alzheimers Dement. 2020;16(7):974–82.
38. Finnema SJ, Rossano S, Naganawa M, Henry S, Gao H, Pracitto R, et al. A single-center, open-label positron emission tomography study to evaluate brivaracetam and levetiracetam synaptic vesicle glycoprotein 2A binding in healthy volunteers. Epilepsia. 2019;60(5):958–67.
39. Holmes SE, Scheinost D, Finnema SJ, Naganawa M, Davis MT, DellaGioia N, et al. Lower synaptic density is associated with depression severity and network alterations. Nat Commun. 2019;10(1):1529.
40. Chen MK, Mecca AP, Naganawa M, Finnema SJ, Toyonaga T, Lin SF, et al. Assessing synaptic density in Alzheimer disease with synaptic vesicle glycoprotein 2A positron emission tomographic imaging. JAMA Neurol. 2018;75(10):1215–24.
41. Van Essen DC, Smith SM, Barch DM, Behrens TE, Yacoub E, Ugurbil K. The WU-Minn human connectome project: an overview. Neuroimage. 2013;80:62–79.
42. Glasser MF, Sotiropoulos SN, Wilson JA, Coalson TS, Fischl B, Andersson JL, et al. The minimal preprocessing pipelines for the Human Connectome Project. Neuroimage. 2013;80:105–24.
43. Cammoun L, Gigandet X, Meskaldji D, Thiran JP, Sporns O, Do KQ, et al. Mapping the human connectome at multiple scales with diffusion spectrum MRI. J Neurosci Methods. 2012;203(2):386–97.
44. van der Weijden CWJ, García DV, Borra RJH, Thurner P, Meilof JF, van Laar PJ, et al. Myelin quantification with MRI: a systematic review of accuracy and reproducibility. Neuroimage. 2021;226:117561.
45. Auvity S, Tonietto M, Caillé F, Bodini B, Bottlaender M, Tournier N, et al. Repurposing radiotracers for myelin imaging: a study comparing 18F-florbetaben, 18F-florbetapir, 18F-flutemetamol,11C-MeDAS, and 11C-PiB. Eur J Nucl Med Mol Imaging. 2020;47(2):490–501.
46. Zeydan B, Lowe VJ, Schwarz CG, Przybelski SA, Tosakulwong N, Zuk SM, et al. Pittsburgh compound-B PET white matter imaging and cognitive function in late multiple sclerosis. Mult Scler. 2018;24(6):739–49.
47. Franzmeier N, Neitzel J, Rubinski A, Smith R, Strandberg O, Ossenkoppele R, et al. Functional brain architecture is associated with the rate of tau accumulation in Alzheimer's disease. Nat Commun. 2020;11(1):347.
48. Desikan RS, Ségonne F, Fischl B, Quinn BT, Dickerson BC, Blacker D, et al. An automated labeling system for subdividing the human cerebral cortex on MRI scans into gyral based regions of interest. Neuroimage. 2006;31(3):968–80.
49. Zheng L, Rubinski A, Denecke J, Luan Y, Smith R, Strandberg O, et al. Combined connectomics, MAPT gene expression, and amyloid deposition to explain regional tau deposition in Alzheimer disease. Ann Neurol. 2024;95(2):274–87.
50 Carroll T, Guha S, Nehrke K, Johnson GVW. Tau post-translational modifications: potentiators of selective vulnerability in sporadic Alzheimer's disease. Biology (Basel). 2021;10(10):1047.
51. Leng K, Li E, Eser R, Piergies A, Sit R, Tan M, et al. Molecular characterization of selectively vulnerable neurons in Alzheimer's disease. Nat Neurosci. 2021;24(2):276–87.
52. Kiani L. Regional vulnerability to Aβ and tau pathology. Nat Rev Neurol. 2024;20(3):133.
53. Olajide OJ, Suvanto ME, Chapman CA (2021) Molecular mechanisms of neurodegeneration in the entorhinal cortex that underlie its selective vulnerability during the pathogenesis of Alzheimer's disease. Biol Open 10(1). https://doi.org/10.1242/bio.056796
54. Yu M, Risacher SL, Nho KT, Wen Q, Oblak AL, Unverzagt FW, et al. Spatial transcriptomic patterns underlying amyloid-β and tau pathology are associated with cognitive dysfunction in Alzheimer's disease. Cell Rep. 2024;43(2):113691.
55. Jack CR Jr, Wiste HJ, Schwarz CG, Lowe VJ, Senjem ML, Vemuri P, et al. Longitudinal tau PET in ageing and Alzheimer's disease. Brain. 2018;141(5):1517–28.
56. La Joie R, Visani AV, Baker SL, Brown JA, Bourakova V, Cha J et al (2020) Prospective longitudinal atrophy in Alzheimer's disease correlates with the intensity and topography of baseline tau-PET. Sci Transl Med 12(524). https://doi.org/10.1126/scitranslmed.aau5732
57. Jacobs HIL, Hedden T, Schultz AP, Sepulcre J, Perea RD, Amariglio RE, et al. Structural tract alterations predict downstream tau accumulation in amyloid-positive older individuals. Nat Neurosci. 2018;21(3):424–31.
58. Fornito A, Arnatkevičiūtė A, Fulcher BD. Bridging the gap between connectome and transcriptome. Trends Cogn Sci. 2019;23(1):34–50.
59. Arnatkeviciute A, Markello RD, Fulcher BD, Misic B, Fornito A. Toward best practices for imaging transcriptomics of the human brain. Biol Psychiatry. 2023;93(5):391–404.
60. Sepulcre J, Grothe MJ, d'Oleire Uquillas F, Ortiz-Terán L, Diez I, Yang HS, et al. Neurogenetic contributions to

amyloid beta and tau spreading in the human cortex. Nat Med. 2018;24(12):1910–8.
61. Montal V, Diez I, Kim CM, Orwig W, Bueichekú E, Gutiérrez-Zúñiga R, et al. Network Tau spreading is vulnerable to the expression gradients of APOE and glutamatergic-related genes. Sci Transl Med. 2022;14(655):eabn7273.
62. Franzmeier N, Dewenter A, Frontzkowski L, Dichgans M, Rubinski A, Neitzel J et al (2020) Patient-centered connectivity-based prediction of tau pathology spread in Alzheimer's disease. Sci Adv 6(48). https://doi.org/10.1126/sciadv.abd1327
63. Nabizadeh F (2023) Initiative ftAsdN. sTREM2 is associated with attenuated tau aggregate accumulation in the presence of amyloid-β pathology. Brain Commun 5(6). https://doi.org/10.1093/braincomms/fcad286
64. Wang J, Huang Q, Chen X, You Z, He K, Guo Q et al (2024) Tau pathology is associated with synaptic density and longitudinal synaptic loss in Alzheimer's disease. Mol Psychiatry. https://doi.org/10.1038/s41380-024-02501-z
65. Wang M, Lu J, Zhang Y, Zhang Q, Wang L, Wu P, et al. Characterization of tau propagation pattern and cascading hypometabolism from functional connectivity in Alzheimer's disease. Hum Brain Mapp. 2024;45(7):e26689.
66. Iaccarino L, Tammewar G, Ayakta N, Baker SL, Bejanin A, Boxer AL, et al. Local and distant relationships between amyloid, tau and neurodegeneration in Alzheimer's disease. Neuroimage Clin. 2018;17:452–64.
67. Ossenkoppele R, Schonhaut DR, Schöll M, Lockhart SN, Ayakta N, Baker SL, et al. Tau PET patterns mirror clinical and neuroanatomical variability in Alzheimer's disease. Brain. 2016;139(Pt 5):1551–67.
68. Dronse J, Fliessbach K, Bischof GN, von Reutern B, Faber J, Hammes J, et al. In vivo patterns of tau pathology, amyloid-β burden, and neuronal dysfunction in clinical variants of Alzheimer's disease. J Alzheimers Dis. 2017;55(2):465–71.
69. Hammond TC, Xing X, Wang C, Ma D, Nho K, Crane PK, et al. β-amyloid and tau drive early Alzheimer's disease decline while glucose hypometabolism drives late decline. Commun Biol. 2020;3(1):352.
70. Levin F, Ferreira D, Lange C, Dyrba M, Westman E, Buchert R, et al. Data-driven FDG-PET subtypes of Alzheimer's disease-related neurodegeneration. Alzheimers Res Ther. 2021;13(1):49.
71. Chang CW, Evans MD, Yu X, Yu GQ, Mucke L. Tau reduction affects excitatory and inhibitory neurons differently, reduces excitation/inhibition ratios, and counteracts network hypersynchrony. Cell Rep. 2021;37(3):109855.
72. Ranasinghe KG, Verma P, Cai C, Xie X, Kudo K, Gao X et al (2022) Altered excitatory and inhibitory neuronal subpopulation parameters are distinctly associated with tau and amyloid in Alzheimer's disease. Elife 11. https://doi.org/10.7554/eLife.77850
73. Fu H, Possenti A, Freer R, Nakano Y, Hernandez Villegas NC, Tang M, et al. A tau homeostasis signature is linked with the cellular and regional vulnerability of excitatory neurons to tau pathology. Nat Neurosci. 2019;22(1):47–56.
74. Rubinski A, Franzmeier N, Dewenter A, Luan Y, Smith R, Strandberg O, et al. Higher levels of myelin are associated with higher resistance against tau pathology in Alzheimer's disease. Alzheimers Res Ther. 2022;14(1):139.
75. Couttas TA, Kain N, Suchowerska AK, Quek LE, Turner N, Fath T, et al. Loss of ceramide synthase 2 activity, necessary for myelin biosynthesis, precedes tau pathology in the cortical pathogenesis of Alzheimer's disease. Neurobiol Aging. 2016;43:89–100.
76. Najm FJ, Madhavan M, Zaremba A, Shick E, Karl RT, Factor DC, et al. Drug-based modulation of endogenous stem cells promotes functional remyelination in vivo. Nature. 2015;522(7555):216–20.
77. Cully M. Neurodegenerative diseases: repurposing for remyelination. Nat Rev Drug Discov. 2015;14(6):383.
78. Mei F, Lehmann-Horn K, Shen YA, Rankin KA, Stebbins KJ, Lorrain DS et al (2016) Accelerated remyelination during inflammatory demyelination prevents axonal loss and improves functional recovery. Elife 5. https://doi.org/10.7554/eLife.18246
79. Green AJ, Gelfand JM, Cree BA, Bevan C, Boscardin WJ, Mei F, et al. Clemastine fumarate as a remyelinating therapy for multiple sclerosis (ReBUILD): a randomised, controlled, double-blind, crossover trial. Lancet. 2017;390(10111):2481–9.
80. Scheff SW, Neltner JH, Nelson PT. Is synaptic loss a unique hallmark of Alzheimer's disease? Biochem Pharmacol. 2014;88(4):517–28.
81. Terry RD, Masliah E, Salmon DP, Butters N, DeTeresa R, Hill R, et al. Physical basis of cognitive alterations in Alzheimer's disease: synapse loss is the major correlate of cognitive impairment. Ann Neurol. 1991;30(4):572–80.
82. Pham E, Crews L, Ubhi K, Hansen L, Adame A, Cartier A, et al. Progressive accumulation of amyloid-beta oligomers in Alzheimer's disease and in amyloid precursor protein transgenic mice is accompanied by selective alterations in synaptic scaffold proteins. Febs j. 2010;277(14):3051–67.
83. Vanhaute H, Ceccarini J, Michiels L, Koole M, Sunaert S, Lemmens R, et al. In vivo synaptic density loss is related to tau deposition in amnestic mild cognitive impairment. Neurology. 2020;95(5):e545–53.
84. Vanderlinden G, Ceccarini J, Vande Casteele T, Michiels L, Lemmens R, Triau E, et al. Spatial decrease of synaptic density in amnestic mild cognitive impairment follows the tau build-up pattern. Mol Psychiatry. 2022;27(10):4244–51.
85. Vogel JW, Corriveau-Lecavalier N, Franzmeier N, Pereira JB, Brown JA, Maass A, et al. Connectome-based modelling of neurodegenerative diseases: towards precision medicine and mechanistic insight. Nat Rev Neurosci. 2023;24(10):620–39.